

**An Instantaneous 3D Ego-Velocity Measurement Algorithm
for Frequency Modulated Continuous Wave (FMCW)
Doppler Radar Data**

by

Carl C. Stahoviak

B.S., Rochester Institute of Technology, 2015

A thesis submitted to the
Faculty of the Graduate School of the
University of Colorado in partial fulfillment
of the requirements for the degree of
Master of Science
Department of Aerospace Engineering Sciences
2020

This thesis entitled:

An Instantaneous 3D Ego-Velocity Measurement Algorithm for Frequency Modulated Continuous Wave (FMCW) Doppler Radar Data

written by Carl C. Stahoviak

has been approved for the Department of Aerospace Engineering Sciences

Prof. Christoffer Heckman

Prof. Christopher Williams

Date _____

The final copy of this thesis has been examined by the signatories, and we find that both the content and the form meet acceptable presentation standards of scholarly work in the above mentioned discipline.

Stahoviak, Carl C. (M.S., Aerospace Engineering)

An Instantaneous 3D Ego-Velocity Measurement Algorithm for Frequency Modulated Continuous Wave (FMCW) Doppler Radar Data

Thesis directed by Prof. Christoffer Heckman

This thesis describes an instantaneous 3D body-frame linear velocity measurement algorithm that operates solely on Doppler radar target data. A robust, model-free estimate of the ego-velocity vector of the sensor platform can be determined from a single radar scan, without requiring additional sensors or target data from previous scans. Additionally, this thesis lays the groundwork for the fusion of this velocity measurement into a visual-inertial-radar Simultaneous Localization and Mapping (SLAM) estimation scheme as a means to augment the traditional limitations of visual-inertial SLAM methods. Real world data sets captured onboard ground and aerial vehicle platforms are evaluated alongside a Vicon motion capture ground truth system. The ego-velocity measurement algorithm takes advantage of the radar's ability to measure both radial velocity, as well as returned signal intensity, and via the incorporation of a statistical re-sampling technique is shown to provide a robust measurement of the 3D body-frame linear velocity components of the sensor platform and their associated measurement uncertainties.

Dedication

Dedicated to William Vincent Stahoviak and Lena Mae Erickson Stahoviak.

"Always remember there was nothing worth sharing like the love that let us share our name."

– Scott Avett

Acknowledgements

First, I would like to acknowledge the contributions of my family, especially my parents John and Amanda Stahoviak who have been a constant source of support throughout my life. I'd like to thank my Mom for her dedication to the educational development of myself and my brothers at a young age. She's been a strong advocate for early-childhood education throughout her adult life, and I'd like to thank her for making that a priority in our lives. I'd like to thank my Dad for being a bonafide nerd – for helping me with math homework and science projects, and for encouraging me to get into electronics and programming in high school. I'd also like to thank him for all the ping-pong matches won and lost over the years. I have such good memories of those games. Finally, I'd like to thank my grandparents, Bill and Lena Stahoviak. Without them, none of this would have been possible.

Next, I would like to acknowledge the contribution of important teachers and mentors in my life, without whom I may never have started down the path I'm on today. Most of all, I'd like to thank Michael Nord. Nord's class was my first introduction to robotics, and it was by far the single most formative educational experience of my life. Thank you, Nord, for creating the best damn classroom and robotics lab that you possibly could have, it has made all the difference in the world for me. I'd like to thank Robert Kraynik for taking me under his wing as a shop employee during my time at RIT. I'd also like to thank Phillip Reu for his mentorship during my time at Sandia Labs. His work on DIC-UQ was my first exposure to measurement uncertainty. Who could have known how important measurement error would become to me years later? Finally, I'd like to thank Chris Heckman and Christopher Williams for their support throughout this entire project.

I'm incredibly grateful for their mentorship. Thank you especially to Chris who went out on a limb and agreed to work with me on my Master's thesis and bring me onto the amazing research group that is the Advanced Robotics and Perception Group (ARPG).

And finally, in the infamous words of Snoop Dogg, *"Last, but not least, I want to thank me. I want to thank me for believing in me. I want to thank me for doing all this hard work... I want to thank me for just being me at all times."*

Contents

Chapter

1	Introduction	1
2	Related Work	4
3	Frequency Modulated Continuous Wave (FMCW) Radar	6
3.1	Radar Signal Processing	6
3.1.1	The Chirp Signal	6
3.1.2	The Radar Data Cube	7
3.2	Experimental Sensor Setup	9
3.2.1	Estimation of Groundtruth	10
4	Methodology	11
4.1	Radar Doppler Velocity Measurement Formulation	11
4.2	Clutter Removal	13
4.3	MLESAC Parameter Estimation & Outlier Rejection	14
4.4	Measurement Model Uncertainties	17
4.4.1	Ordinary Least Squares, OLS	17
4.4.2	Orthogonal Distance Regression, ODR	18
4.4.3	Solving the ODR Problem - Computing the Jacobian	21
4.4.4	Computation of the Asymptotic Covariance Matrix	23
4.4.5	The ODR Algorithm	25

5	Results	27
5.1	Simulation Study	27
5.2	2D Radar Data - Static Environment	29
5.3	2D Radar Data — Semi-dynamic Environment	30
5.4	3D Radar Data — Static Environment	32
6	Conclusion	35
Bibliography		38

Appendix

A	Orthogonal Distance Regression, A Poem	41
	Orthogonal Distance Regression	41

Tables

Table

5.1	Simulation Study — Velocity Profile Estimation	28
5.2	2D Radar Data — Static Environment	30
5.3	2D Radar Data — Semi-Dynamic Environment	32
5.4	3D Radar Data — Static Environment	33

Figures

Figure

3.1	The FMCW chirp signal [11]	7
3.2	The radar data cube [21]	9
4.1	Radar target frame coordinate geometry and sensor coordinate frame	13
4.2	Spurious target data in the form of radar clutter	14
4.3	MLESAC velocity profile estimation	16
4.4	2D Orthogonal Distance Regression (ODR) $k\sigma$ confidence bounds.	25
4.5	2D Orthogonal Distance Regression (ODR) covariance values, $[\sigma_{v_x}, \sigma_{v_y}]$	25
5.1	Experimental vehicle platforms with custom sensor rigs consisting of 77–81 GHz FMCW radar, Intel RealSense camera and microstrain IMU.	27
5.2	MLESAC outlier rejection and ODR velocity profile estimation	28
5.3	2D Orthogonal Distance Regression (ODR) velocity vector measurement for a static environment. Also noted are time at which the Vicon motion-capture system is momentarily unreliable.	29
5.4	2D Orthogonal Distance Regression (ODR) velocity vector measurement for a semi-dynamic environment. Dashed red lines – – indicate time intervals during which a person was moving in the scene.	31
5.5	3D Orthogonal Distance Regression (ODR) velocity vector measurement for a static environment.	33

5.6 3D Orthogonal Distance Regression (ODR) measurement uncertainties	34
---	----

Chapter 1

Introduction

The field of *Simultaneous Localization and Mapping* (SLAM) has been an active area of research since the early work of Cheeseman on the representation and estimation of spatial uncertainty [26] [25], followed soon after by the early work of Newman that directly addressed the SLAM problem [8]. There exist several dominant SLAM implementations including Extended Kalman Filter SLAM (EKF-SLAM), Particle Filter SLAM (FastSLAM), and more recently, graph optimization SLAM, GraphSLAM [24]. The scope of these implementations has spanned varying degrees of environment uncertainty and a multitude of sensing modalities including GPS, cameras, LiDARs, radars, IMUs and their various combinations.

Intrinsic to the SLAM problem is the estimation of state, including a robot's current and past pose information as well as the position of landmarks in its environment. Numerous methods, including those mentioned above, have been proposed to solve this problem, most of which rely on *sensor fusion*, or the combination of measurements from complementary sensors. For instance, cameras provide information on structure and motion, but rely on environmental factors such as the availability of light and texture to infer structure; inertial measurement units (IMU) on the other hand provide spatio-temporal constraints but cannot provide information on structure. Measurements from both of these sensors can be fused to simultaneously estimate a robot's motion and environment in a process known as visual-inertial SLAM (VI-SLAM). There are two significant shortcomings in this approach:

- (1) Integrating IMU data into relative pose constraints requires an estimate of the robot's

linear velocity; visual and inertial sensors do not provide a way to measure linear velocity directly.

- (2) Cameras are highly susceptible to motion blur and visual occlusions such as fog and dust; when visual tracking is lost, IMU-based velocity estimates can become very noisy. This can have catastrophic consequences for the estimation scheme.

Due to these two critical shortcomings, it is highly desirable to employ a sensor that would serve to constrain velocity by direct measurement and which does not share the failure modes of cameras. One possible option would be to implement a sort of radar odometry, which would track radar targets in a static scene and estimate ego-motion through space, thereby implicitly measuring velocity. Such an approach could result in errors associated with target matching (data association) across frames to estimate odometry, and would not serve to constrain velocity through a direct measurement. Another option for addressing these two critical shortcomings is to fuse 3D Doppler radar measurements via the use of a frequency-modulated continuous wave (FMCW) radar sensor.

While radar is well-established in the automotive industry and has been used for various tasks in vehicle autonomy, including collision avoidance, automated braking, lane keeping, autonomous parking, etc. [9], only a very limited number of methodologies for using radar as a primary sensor for ego-motion estimation have been presented in the literature. With the recent development of patch-antenna system-on-chip (SoC) radar sensors, these techniques are taking on greater significance. This type of FMCW millimeter-wave radar sensor has no moving parts and is advantageous for several reasons [5]:

- (1) Radar exhibits good signal penetration in adverse atmospheric and lighting conditions, e.g. rain, snow, fog, dust and low-light conditions.
- (2) Radar can resolve targets in both azimuth and elevation with a typical field-of-view similar to significantly more expensive LiDAR sensors.

- (3) Radar has operating parameters that may be scaled for both long and short range applications in software.

A significant challenge remains in fusing these data with traditional SLAM methods. The radial velocity measurements produced by these sensors correspond to distinct *targets* in a given radar scan, and these multiple measurements must be aggregated to produce single, robust ego-velocity measurement, preferably without relying on additional sensors or radar data from previous scans.

This thesis is organized as follows: Chapter 2 reviews related work. An overview of radar signal processing and a description of the sensor setup onboard the experimental vehicle platforms is given in Chapter 3. The problem formulation and methodology are presented in Chapter 4. This chapter describes an algorithm for the measurement of the sensor platform's 3D ego-velocity vector that employs statistical resampling and a form of *error-in-variables* regression analysis. This description lays the foundation for the inclusion of this velocity measurement into any number of state estimation techniques that employ sensor fusion, e.g. a visual-inertial-radar SLAM framework. Next, Chapter 5 presents results for both ground vehicle and aerial vehicle platforms. This approach is particularly developed with agricultural or subterranean applications in mind where darkness and dust are prevalent and foul visual data, but the author envisions a range of other interesting applications as well.

Chapter 2

Related Work

In recent years, significant progress has been made in the use of radar for ego-motion estimation. In 2016, Schuster et al. presented a methodology [22] by which a radar feature detector and descriptor combination [20] is used to produce landmarks from the incoming radar data and generate a map of the environment using the GraphSLAM algorithm. This approach relied on non-Doppler radar, IMU and wheel encoder data and demonstrated a mean localization error of approximately 1m for optimized maps, and a matching error between landmarks and the ground truth with a mean of 6.8cm.

In 2018, Cen and Newman published a method by which motion estimation is achieved via a radar-only technique [8]. Their methodology extracts radar landmarks from the power-spectra signal of a rotating scanning radar. A scan matching algorithm that attempts to extract the rigid-body motion that will best align the extracted features from successive radar scans is then used to derive the motion estimate. It should be noted that this method also employs non-Doppler radar.

Kellner et al. have developed methods [16, 17] by which the velocity vector and orientation of a moving vehicle can be estimated using Doppler radar. These methods implement an outlier rejection technique and derive an estimate of the velocity vector of an external moving vehicle via a form of total least-squares regression analysis. The radar-based ego-velocity estimation algorithm implemented in this thesis extends this particular type of regression analysis to vector-valued explanatory variables, as well as incorporates a log-likelihood outlier rejection method and a radar-specific weighting scheme to derive an ego-motion estimate rather than an estimate of an external

vehicle's motion.

Additionally, methods for aerial vehicle based velocity estimation have spanned the spectrum from pure visual (e.g. optical flow) to inertial-only techniques [15, 1, 18]. For those methods that rely on visual data, the quality of the body-frame velocity estimate is quickly degraded in low-light and other feature-poor environments such those encountered in subterranean operations.

Chapter 3

Frequency Modulated Continuous Wave (FMCW) Radar

3.1 Radar Signal Processing

The Frequency Modulated Continuous Wave (FMCW) radar used in this work is a solid-state Multiple In Multiple Out (MIMO) patch antenna radar system consisting of two pairs of transmit antenna elements and four receive antenna elements. The following sections describe the method by which the so-called *radar data cube* is constructed and how information on target range, bearing and Doppler (radial) velocity is extracted from the data cube. Next, an overview of the data produced by the particular FMCW radar sensor used in this work is given.

3.1.1 The Chirp Signal

The processed FMCW radar target data includes the target location in polar coordinates, the distance r_i , azimuth θ_i , and elevation ϕ_i , as well the Doppler velocity and a target intensity measure I_i (in dB) that is proportional to the signal-to-noise (SNR) ratio of the target. How does the radar make measurements of these quantities, in particular, the range, bearing and Doppler velocity of a given set of targets?

At the heart of FMCW radar signal processing is a frequency modulated signal called a *chirp*. A chirp is a sinusoid whose frequency *linearly* increases with time. The transmitted chirp signal is characterized in the frequency domain by the bandwidth that the chirp sweeps (B) measured in GHz, and the duration of the chirp T_c typically measured in microseconds. These parameters define the frequency slope of the chirp signal where the slope is given by $s = B/T_c$. The chirp signal

is illustrated in Fig. 3.1. The basic unit of transmission of an FMCW radar consists of N such chirps and is referred to in radar signal processing literature as a *frame*. The transmitted frame of chirps is propagated forward, reflected off one or more targets in the scene and then received by the receive antenna element(s). The transmit and receive signals are then mixed and low-pass filtered. The resulting signal (referred to as the *intermediate frequency* signal) will be a sinusoid with a beat frequency given by $f_{beat} = sT_d$, where s is the slope [GHz/microsecond] and T_d is the roundtrip delay time of the propagated wave. Thus, the time-delay of the signal to propagate out-and-back from the target is related to the target range, and is proportional to the measured beat frequency. The following section describes the process by which target range, bearing and Doppler velocity are calculated via the fast Fourier Transform (FFT) which converts the received data into range-amplitude, velocity-amplitude and angle-amplitude space.

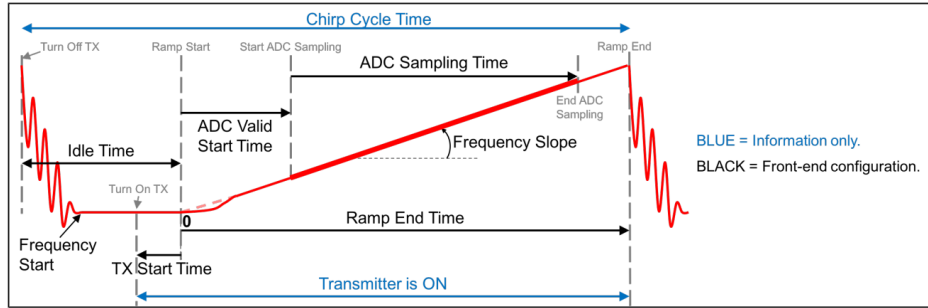


Figure 3.1: The FMCW chirp signal [11]

3.1.2 The Radar Data Cube

The concept of the radar *data cube* is introduced as a convenient way to represent a collection of received radar signals built up sample-by-sample in time and space. Once the received data has been assembled into this format, discrete FFTs along different dimensions of the data cube can be used to extract range, bearing and Doppler velocity information corresponding to each target in the scan. Constructing the radar data cube happens in three steps.

First, consider the case of a single transmitted chirp. As mentioned previously, the received

signal is mixed with the transmit signal and low-pass filtered resulting in the intermediate frequency signal. The intermediate frequency signal consists of the super-position of all target generated intermediate frequencies. The intermediate frequency signal is sampled by the ADC and an FFT on this time-domain signal is able to resolve the frequency components corresponding each range bin. Each frequency bin is often referred to as a *range bin*, and the number of range bins determines the size of the y-axis of the data cube (shown in Fig. 3.2 as N_{ADC}). In radar literature, this is often referred to as the *fast-time* dimension because the sampling time rate tends to be fairly high – sampling rates in the MHz are common. A fast-time ADC sampling rate of around 7 MHz is typical for this particular sensor. Thus, the discrete FFT on the time-domain sampled signal converts the beat frequencies of the intermediate frequency signal into a range-amplitude frequency-domain signal. The frequencies of various peaks in the range-amplitude signal corresponding to discrete range bins are used to estimate the distance of the target(s).

The next dimension of the radar data cube is defined by the frame duration which is directly proportional to the number of chirps transmitted per frame, N . The number of transmitted chirps per frame are referred to as the *Doppler bins*, and the Doppler velocity resolution of the sensor is directly proportional to the frame duration, i.e. the number of transmitted chirps per frame. This dimension of the radar data cube is often referred to as the *slow-time* dimension, as the total frame duration is often on the order of several milliseconds (much slower than the range gate sampling frequency). A discrete FFT across the series of chirps in a frame is referred to as the Doppler-FFT and can be used to estimate the Doppler velocity of distinct targets. The Doppler-FFT is performed for each range bin across the N transmitted chirps, and thus the range-FFT must be performed for every chirp in the frame prior to the Doppler-FFT processing being performed.

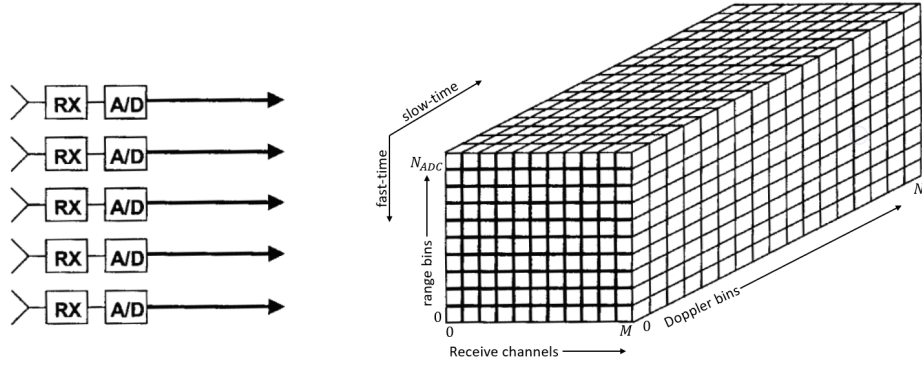


Figure 3.2: The radar data cube [21]

Now, the concept of the 2D-FFT can be introduced. The 2D-FFT calculation consists of performing the range-FFT for each chirp in the transmitted frame followed by the Doppler-FFT across the N transmitted chirps. Thus, for a given transmit and receive pair, there will be a range-Doppler matrix of size $N_{ADC} \times N$. For a given frame, the 2D-FFT is performed for each transmit-receive pair. Each transmit-receive pair forms a channel, and with two transmitters and four receivers, there are 8 unique channels spatially distributed across the antenna aperture. These 8 channels define the x-dimension of the radar cube. A constant-false-alarm-rate (CFAR) threshold is applied to the signal-to-noise ratio of each target identified in the 2D-FFT. Spatially sampling the receive signals across these channels allows for the determination of target bearing in a process known as the Angle-FFT. Due to the memory constraints of the system, the Angle-FFT is only performed for those range-angle bins that have passed the CFAR threshold criteria. Note that the 2D-FFT matrix must exist for each transmit-receive pair before the Angle-FFT can be performed.

3.2 Experimental Sensor Setup

The algorithm described in the following sections has been developed to operate on data produced by a radar-on-chip radar sensor whose detection axes have been rigidly aligned with the body-frame axes of ground and quadrotor vehicle platforms. The sensor operates in 3D (determined by the physical layout of the transmitter-receiver pairs) and has a field-of-view (FOV) of approximately ± 75 degrees azimuth and ± 20 degrees elevation. The radar operates in the 77-81

GHz band. Several parameters of interest including the maximum range of the sensor, the range resolution, the velocity resolution, as well as the maximum unambiguous radial velocity measurable are all defined by the so-called *chirp parameters* of the radar. These parameters define the profile of the transmitted frequency modulated signal as well as the frame duration, and can be tuned (with various trade-offs in mind) to achieve the desired sensor behavior. In the configuration that yields the highest velocity resolution, the sensor produces targets at a maximum range of 11.2 m at a resolution of 12.5 cm, and a maximum Doppler (radial) velocity of 2.56 m/s at a resolution of 0.044 m/s.

The sensor produces a maximum of 300 targets per scan at a rate of 10 Hz. As mentioned in the preceding section, the processed data includes the target location in polar coordinates, the distance r_i , azimuth θ_i , and elevation ϕ_i , as well the Doppler velocity and a target intensity measure I_i (in dB) that is proportional to the signal-to-noise (SNR) ratio (sometimes referred to as signal-to-clutter ratio) of the target.

3.2.1 Estimation of Groundtruth

To estimate groundtruth pose and velocity of the sensor platform that are spatially and temporally aligned with the sensor platform’s coordinate frame, we use measurements from a Vicon motion capture system and an IMU onboard the vehicle platforms. The Vicon system provides drift-free pose measurements. However, the transform between the Vicon system’s coordinate frame and the vehicle’s coordinate frame is unknown. Additionally, the Vicon measurements are subject to both noise and communication latency between the Vicon system and the host system. Thus, IMU measurements are used to estimate the transform between the Vicon coordinate frame and the vehicle’s body-frame, the timestamp offsets between the Vicon system and host system, and to smooth noise in the Vicon measurements. This is similar to the method used to estimate groundtruth in [6], where clock biases are estimated as part of the measurement matching process due to the random delay induced by WiFi transmission.

Chapter 4

Methodology

The aim of this work is to develop an instantaneous 3D body-frame linear velocity measurement algorithm that operates solely on radar target data. A robust estimate of the ego-velocity vector of the sensor platform can be determined for a single radar scan, without requiring additional sensors or target data from previous scans.

Radar target data is binned according the spatial resolution (range resolution and angle resolution) and radial velocity resolution of the sensor as described in detail in Ch. 3.1.2. A clustering algorithm can be applied to one or more of these dimensions to combine measurements that can likely be attributed to the same target. A clustering algorithm like DBSCAN [10] that makes no assumption about the number of clusters in the data can be applied in post-processing to the radar target data for this task. Another approach is to cluster measurements in pre-processing based on peaks of the neighboring range and Doppler bins. It is assumed from here on in that the target data generated by the sensor for a given radar scan has been clustered in Doppler space.

4.1 Radar Doppler Velocity Measurement Formulation

The Doppler velocity measurement produced by the radar for a given target is equal to the magnitude of the projection of the relative velocity vector onto the line \mathbf{R} defined between sensor origin and the target location, i.e. radar Doppler is a measure of the line-of-sight (radial) relative motion between the sensor and the target. In general, the Doppler velocity of target i can be

expressed as

$$v_{r,i} = \left(\frac{\mathbf{R}_i}{\|\mathbf{R}_i\|} \right) \cdot \mathbf{v}_{rel} \quad (4.1)$$

We will assume that every target in the scene is stationary, and that only the sensor platform is moving. One expected benefit of the MLESAC implementation (Sec. 4.3) is a means by which dynamic agents in the environment can be effectively handled and treated as outliers in the body-frame velocity estimation problem. Assuming target i is stationary and that the sensor is aligned with the body-frame axes, Eq. (4.1) can be re-written as

$$v_{r,i} = \left(\frac{\mathbf{R}_i}{\|\mathbf{R}_i\|} \right) \cdot \mathbf{v}^b = \begin{bmatrix} \cos \theta_i \cos \phi_i \\ \sin \theta_i \cos \phi_i \\ \sin \phi_i \end{bmatrix}^T \begin{bmatrix} v_x \\ v_y \\ v_z \end{bmatrix}^b, \quad (4.2)$$

where \mathbf{v}^b denotes the body-frame velocity of the sensor platform with components $[v_x, v_y, v_z]^T$, and the azimuth and elevation of the target's polar coordinates are θ_i and ϕ_i , respectively. The radar target geometry is defined in Fig. 4.1. Restating Eq. (4.2), we can express the Doppler velocity as $v_{r,i} = v_x \cos \theta_i \cos \phi_i + v_y \sin \theta_i \cos \phi_i + v_z \sin \phi_i$, referred to as the *velocity profile*, which defines a sinusoidal *surface* in (θ, ϕ, v_r) space. The 3D ego-velocity estimation problem can now be posed as an over-determined non-linear system of equations where each unique equation corresponds to a target $i = 1, \dots, n$ in the scan:

$$\begin{bmatrix} v_{r,1} \\ v_{r,2} \\ \vdots \\ v_{r,n} \end{bmatrix} = \begin{bmatrix} \cos \theta_1 \cos \phi_1 & \sin \theta_1 \cos \phi_1 & \sin \phi_1 \\ \cos \theta_2 \cos \phi_2 & \sin \theta_2 \cos \phi_2 & \sin \phi_2 \\ \vdots & \vdots & \vdots \\ \cos \theta_n \cos \phi_n & \sin \theta_n \cos \phi_n & \sin \phi_n \end{bmatrix} \begin{bmatrix} v_x \\ v_y \\ v_z \end{bmatrix} \quad (4.3)$$

,

or $\mathbf{v}_r = M(\theta, \phi)\mathbf{v}^b$. Eq. (4.3) generally has a unique solution $[v_x, v_y, v_z]^T$ when three distinct targets are identified, and is over-constrained for more than three targets. Doppler velocity is a measure

of radial velocity, and thus, for a given target, motion in the plane normal to \mathbf{R}_i is completely unobservable by the radar. As such, the body-frame velocity of the platform cannot be solved for less than three distinct target observations at distinct azimuth and elevation locations. Due to the binning of angle-of-arrival data, the matrix M will be singular when the sum of the number of azimuth and elevation bins associated with three distinct targets is less than five.

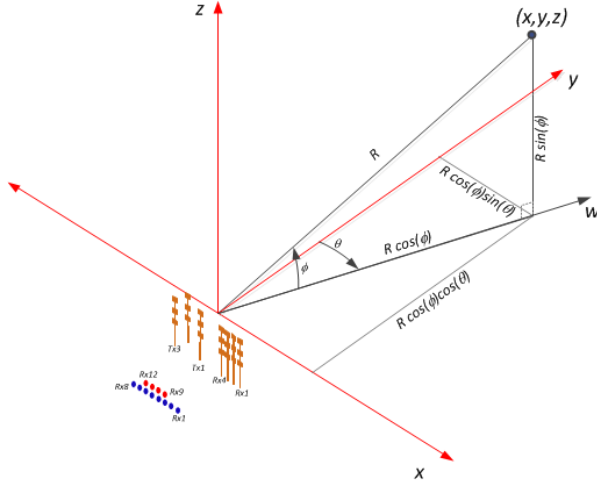


Figure 4.1: Radar target frame coordinate geometry and sensor coordinate frame

The method for solving Eq. (4.3) is as follows. First, spurious target data that can be attributed to antenna interference at the sensor plane are removed from the target set. Next, Maximum Likelihood Sample and Consensus (MLESAC) [29] is employed to derive a first-pass estimate of the ego-velocity profile parameters as well as identify an inlier set of targets that is free of targets adversely affected by significant sensor noise and other radar-specific corruptions of data, e.g. multipath reflections. Finally, a total least-squares regression analysis is seeded with the MLESAC velocity profile estimate and a precise estimate of the ego-velocity vector is derived from the MLESAC inlier set.

4.2 Clutter Removal

Experiments with this particular type of patch-antenna radar have shown that the radar target data will contain spurious, persistent data points that are an artifact of signal interference

at the sensor plane, otherwise referred to as *clutter*. These spurious targets (shown in red in Fig. 4.2) have several identifying features that will allow them to be removed from further processing. These targets will have a time-invariant intensity value and always show up in the zero-Doppler bin. A combination of thresholding in intensity and Doppler space can be used to effectively remove these targets from the scan.

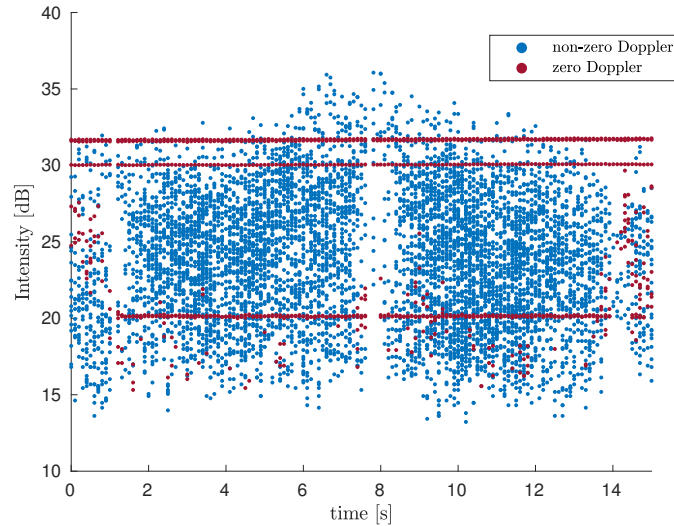


Figure 4.2: Spurious target data in the form of radar clutter

4.3 MLESAC Parameter Estimation & Outlier Rejection

Random Sample and Consensus (RANSAC) [12] is a non-deterministic, iterative method to estimate the parameters of a mathematical model from a set of observed data points that contains outliers, where outliers are to be afforded no influence on the value of the parameter estimate. RANSAC iteratively resamples from a set of observed data to determine a consensus hypothesis from the set, and is commonly used as an outlier rejection technique.

Maximum Likelihood Estimation Sample and Consensus (MLESAC) [29] adopts the same sampling strategy as RANSAC, but determines a parameter estimate that maximizes the data log-likelihood function rather than maximizing the cardinality of the inlier set, i.e. the number of data points ascribed to the inlier set. Through the use of a user-defined threshold on the *distance* from

an observed data point to the velocity profile surface, a determination of the inlier and outlier sets is made.

Let us revisit the assumption that ϵ_i , the error associated with the radar's measurement of a target's Doppler velocity, is a zero-mean Gaussian random variable, $\epsilon_i \sim \mathcal{N}(0, \sigma_{v_r}^2)$. In general, the log of the likelihood function for a given observation set \mathbf{X} of a Gaussian random variable $x \sim \mathcal{N}(\mu, \sigma^2)$ is given by

$$\log P(\mathbf{X}|\mu, \sigma^2) = \log \prod_{i=1}^N \mathcal{N}(x_i|\mu, \sigma^2) \quad (4.4)$$

For the case of the radar Doppler velocity generative model, the data log-likelihood function can be expressed as

$$\log P(\mathbf{v}_r|\boldsymbol{\beta}) = \log \prod_{i=1}^N \frac{1}{(2\pi\sigma_{v_r}^2)^{1/2}} \cdot \exp \left\{ -\frac{1}{2\sigma_{v_r}^2} (f([\theta_i, \phi_i]^T; \boldsymbol{\beta}) - v_{r,i})^2 \right\} \quad (4.5)$$

where $\epsilon_i = f([\theta_i, \phi_i]^T; \boldsymbol{\beta}) - v_{r,i}$ and $\sigma_{v_r} = 0.044$ m/s. The measurement model f is defined by Eq. (4.2) and the parameter vector to be estimated by MLSEAC is $\boldsymbol{\beta} = [v_x, v_y, v_z]^T$, the 3D body-frame velocity vector of the sensor platform. What follows is a derivation of the final form of the data log-likelihood, $\log P(\mathbf{v}_r|\boldsymbol{\beta})$.

$$= \log \left[\left(\frac{1}{2\pi\sigma_{v_r}^2} \right)^{N/2} \cdot \left(\exp \left\{ -\frac{1}{2\sigma_{v_r}^2} \epsilon_1^2 \right\} \times \cdots \times \exp \left\{ -\frac{1}{2\sigma_{v_r}^2} \epsilon_N^2 \right\} \right) \right] \quad (4.6)$$

$$= \frac{N}{2} \log \left(\frac{1}{2\pi\sigma_{v_r}^2} \right) + \log \left[\exp \left\{ -\frac{1}{2\sigma_{v_r}^2} \epsilon_1^2 \right\} \times \cdots \times \exp \left\{ -\frac{1}{2\sigma_{v_r}^2} \epsilon_N^2 \right\} \right] \quad (4.7)$$

$$= \frac{N}{2} (\log(1) - \log(2\pi\sigma_{v_r}^2)) + \log \left[\exp \left\{ -\frac{1}{2\sigma_{v_r}^2} \epsilon_1^2 \right\} \right] + \cdots + \log \left[\exp \left\{ -\frac{1}{2\sigma_{v_r}^2} \epsilon_N^2 \right\} \right] \quad (4.8)$$

$$= -\frac{N}{2} \log(2\pi) - \frac{N}{2} \log(\sigma_{v_r}^2) - \frac{1}{2\sigma_{v_r}^2} \sum_{i=1}^N \epsilon_i^2 \quad (4.9)$$

Disregarding the first two constant terms, we can express the data log-likelihood as

$$\log P(\mathbf{v}_r | \boldsymbol{\beta}) = -\frac{1}{2\sigma_{v_r}^2} \sum_{i=1}^N (f([\theta_i, \phi_i]^T; \boldsymbol{\beta}) - v_{r,i})^2 \quad (4.10)$$

For the case of normally distributed zero-mean errors, maximizing the data log-likelihood function results in minimizing the ordinary least squares (OLS) problem. To evaluate the performance of the MLESAC algorithm, a set of simulated 2D radar Doppler measurements are generated with outliers. Figure 4.3a demonstrates that the MLESAC velocity profile estimate is robust to the presence of outliers and is able to recover a reliable estimate of the true velocity profile parameters. Also important to note in Fig. 4.3a is the mis-classification of several inlier data points (near the bottom left of the figure) as outliers. This is a direct result of choosing a distance threshold that is too small. A result such as the one shown can be easily mitigated by appropriately tuning the distance parameter for the particular application of MLESAC. It can be seen in Fig 4.3b that the data log-likelihood function is strictly increasing with each iteration of the MLESAC algorithm.

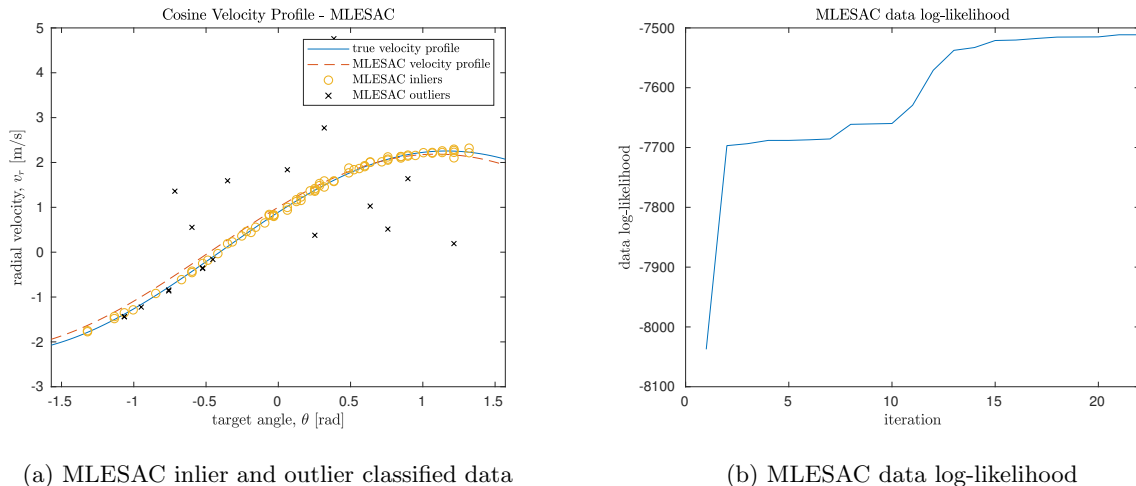


Figure 4.3: MLESAC velocity profile estimation

4.4 Measurement Model Uncertainties

For any given target in a radar scan, the Doppler velocity and bearing measurements produced by the radar are affected by both sensor noise and the binning process previously described Ch. 3, resulting in uncertainty in both the *explanatory* and *independent* variables. There exist numerous methods for appropriately dealing with measurement errors [14], Ordinary Least Squares (OLS) being among the most well-known. A brief review of OLS is provided below as an introduction to a method of *total* least squares regression analysis that is better suited to dealing with the errors in multiple observed variables as is the case for the radar Doppler measurement model.

4.4.1 Ordinary Least Squares, OLS

Least squares is arguably the standard method for fitting data to a model when there are errors in the observations. Consider the data pairs (x_i, y_i) , $i = 1, \dots, n$ where x_i and y_i are both observed random variables such that the relationship between y_i and x_i can be defined by a smooth and possibly nonlinear function f

$$y_i = f(x_i; \boldsymbol{\beta}) \quad (4.11)$$

where $\boldsymbol{\beta} \in \mathbb{R}^p$ is the parameter vector to be estimated. If there are no errors in either x_i or y_i and if $\boldsymbol{\beta}$ is known exactly then Eq. 4.11 holds true. In classical least squares, it is assumed that x_i is known exactly and that y_i is observed with error. In this particular application (and in general) x_i is also observed with error. These errors can reasonably be ignored and a reliable estimate of $\boldsymbol{\beta}$ can be computed if they are smaller relative to errors in y_i . Assuming that errors in y_i are given by the normally distributed zero-mean random variable $\epsilon_i \sim \mathcal{N}(0, \sigma_y)$, we have that

$$y_i + \epsilon_i = f(x_i; \boldsymbol{\beta}) \quad (4.12)$$

and the parameter set $\boldsymbol{\beta}$ can be estimated via the classical, or ordinary, least squares (OLS)

minimization given by

$$\boldsymbol{\beta}^* = \arg \min_{\boldsymbol{\beta}} \sum_{i=1}^n \|\epsilon_i\|^2 = \arg \min_{\boldsymbol{\beta}} \sum_{i=1}^n \|f(x_i; \boldsymbol{\beta}) - y_i\|^2 \quad (4.13)$$

This can be interpreted as minimizing the sum of the squares of the *vertical distances* from the observed data points to the curve $y = f(x; \boldsymbol{\beta})$.

4.4.2 Orthogonal Distance Regression, ODR

To address the induced uncertainty in range, bearing and Doppler measurements, we employ Orthogonal Distance Regression (ODR), a total least squares regression method for "finding the maximum likelihood estimators of parameters in measurement error models in the case of normally distributed errors" [4]. Specifically, we make use of the stable and efficient algorithm of Boggs, Byrd and Schnabel [2] to derive an estimate of the velocity profile parameters when the underlying model is assumed to be nonlinear in either the measured variables, the parameters or both.

In general, the measurement error model associated with ODR can be stated by first defining $\mathbf{X}_i = [\theta_i, \phi_i]^T$ and $Y_i = v_{r,i}$, $i = 1, \dots, n$ as observed random variables with underlying true values $\mathbf{x}_i = [\bar{\theta}_i, \bar{\phi}_i]^T$ and $y_i = \bar{v}_{r,i}$, $i = 1, \dots, n$, respectively. Here, $\mathbf{x}_i \in \mathbb{R}^m$ and $y_i \in \mathbb{R}$. We assume that $\boldsymbol{\delta}_i \in \mathbb{R}^m$ and $\epsilon_i \in \mathbb{R}$ are the zero-mean Gaussian random errors associated with \mathbf{x}_i and y_i , respectively, such that $\mathbf{X}_i = \mathbf{x}_i + \boldsymbol{\delta}_i$ and $Y_i = y_i + \epsilon_i$. We define the observation model f as a smooth nonlinear function such that $Y_i = f(\mathbf{X}_i + \boldsymbol{\delta}_i; \boldsymbol{\beta}) - \epsilon_i$. ODR seeks to estimate the parameter set $\boldsymbol{\beta}$ by accounting for the fact that both \mathbf{X}_i and Y_i are observed with error. This is done by minimizing the sum of the squares of the *orthogonal distances* (as opposed to the vertical distance in OLS) from the data point (\mathbf{X}_i, Y_i) to the surface $y = f(\mathbf{x}; \boldsymbol{\beta})$. Thus, $\boldsymbol{\beta}$ is the solution of the constrained minimization problem:

$$\boldsymbol{\beta}^* = \arg \min_{\boldsymbol{\beta}, \boldsymbol{\delta}, \boldsymbol{\epsilon}} \sum_{i=1}^n (\epsilon_i^2 + \boldsymbol{\delta}_i^2), \quad (4.14a)$$

$$\text{subject to: } Y_i = f(\mathbf{X}_i + \boldsymbol{\delta}_i; \boldsymbol{\beta}) - \epsilon_i. \quad (4.14b)$$

The constraint given by Eq. (4.14b) can be used to eliminate ϵ_i from Eq. (4.14a), and allowing for a weighting scheme to be applied to the observed data points, the unconstrained minimization problem, otherwise referred to as the *weighted* ODR problem, can be defined as

$$\boldsymbol{\beta}^* = \arg \min_{\boldsymbol{\beta}, \boldsymbol{\delta}} \sum_{i=1}^n w_i^2 \left(\left[f(\mathbf{X}_i + \boldsymbol{\delta}_i; \boldsymbol{\beta}) - Y_i \right]^2 + \boldsymbol{\delta}_i^T D_i^2 \boldsymbol{\delta}_i \right), \quad (4.15)$$

where $w_i \geq 0, i = 1, \dots, n$ are the weights associated with each data point and $D_i = \text{diag}\{d_{ij} > 0, j = 1, \dots, m\}$ is a diagonal matrix of order m with diagonal entries $d_{ij} = \sigma_{\epsilon_i}/\sigma_{\delta_i}$ referred to as the *error variance ratios*. In algorithm 869: ODRPACK95 [30], the most current implementation of weighted ODR with bound constraints, a constant weighting scheme is assumed such that $w_i = 1/\sigma_{\epsilon_i}$.

The target data generated by the radar contains measurements of azimuth angle, elevation angle and the Doppler velocity such that all three quantities are observed with error. It is assumed that these errors are distributed as zero-mean additive Gaussian white noise processes such that the diagonal matrix D_i can be defined in terms of the error variance ratios d_{ij} as:

$$D_i = \begin{bmatrix} \frac{\sigma_{v_r}}{\sigma_{\theta_i}} & 0 \\ 0 & \frac{\sigma_{v_r}}{\sigma_{\phi_i}} \end{bmatrix}, \quad (4.16)$$

where σ_{v_r} is defined by the aforementioned chirp parameters and is known to be $\sigma_{v_r} = 0.044$ m/s. The azimuth and elevation binning of the radar is such that the angular bins are not evenly distributed across the FOV, but instead the angular resolution is higher for azimuth and elevation angular locations nearest boresight and the angular resolution degrades proportional to the angle-off-boresight. As such, azimuth and elevation uncertainty, σ_{θ_i} and σ_{ϕ_i} , respectively, can be most accurately expressed as a function of the target's angular coordinates, but to make the implementation of ODR more manageable, empirically-derived, average, constant values of $\sigma_\theta = 2.44^\circ$ and $\sigma_\phi = 2.36^\circ$ will be used, and the error variance ratio matrix can now be expressed as a target-

independent quantity

$$D = \begin{bmatrix} \frac{\sigma_{v_r}}{\sigma_\theta} & 0 \\ 0 & \frac{\sigma_{v_r}}{\sigma_\phi} \end{bmatrix}. \quad (4.17)$$

Additionally, the radar target data consists of an intensity measurement I_i (in dB) that is proportional to the radar-cross-section (RCS) of the target. This intensity measure is a function of the target's radar reflectivity and can be influenced by factors including material type and density, surface roughness, object shape, and the angle at which a target is viewed. In general, false targets that can be attributed to noise will typically fall below a certain intensity threshold, while real, persistent targets will have a higher intensity value. A weighting scheme that takes into account the target's normalized intensity value can be used to improve the ODR estimate of the velocity profile parameters, with weights defined as

$$w_i = \frac{\text{normalized}(I_i)}{\sigma_{v_r}}. \quad (4.18)$$

We can now pose the 3D body-frame linear velocity estimation problem as a weighted ODR problem of the form

$$\begin{bmatrix} v_x \\ v_y \\ v_z \end{bmatrix}^* = \arg \min_{\beta, \delta} \sum_{i=1}^n w_i^2 \left\{ \left(\begin{bmatrix} \cos(\theta_i + \delta\theta_i) \cos(\phi_i + \delta\phi_i) \\ \sin(\theta_i + \delta\theta_i) \cos(\phi_i + \delta\phi_i) \\ \sin(\phi_i + \delta\phi_i) \end{bmatrix}^T \begin{bmatrix} v_x \\ v_y \\ v_z \end{bmatrix} - v_{r,i} \right)^2 + \boldsymbol{\delta}_i^T D^2 \boldsymbol{\delta}_i \right\}, \quad (4.19)$$

with a weighting scheme and error variance ratio matrix as described above. It follows that the vectors $\mathbf{v}_r, \mathbf{w} \in \mathbb{R}^n$, $\mathbf{X} = [\theta_1, \phi_1, \theta_2, \phi_2, \dots, \theta_n, \phi_n]^T$, $\boldsymbol{\delta} = [\delta\theta_1, \delta\phi_1, \delta\theta_2, \delta\phi_2, \dots, \delta\theta_n, \delta\phi_n]^T \in \mathbb{R}^{nm}$, and the parameter vector $\boldsymbol{\beta} = [v_x, v_y, v_z]^T \in \mathbb{R}^p$. By exploiting the particular structure of the ODR problem, the computational complexity of the algorithm can be reduced to $O(np^2) + O(nm)$, which differs only marginally from the computational complexity of the OLS problem, $O(np^2)$. We make use of the ODR implementation described in [30], which converges in typically 4–6 iterations.

4.4.3 Solving the ODR Problem - Computing the Jacobian

Orthogonal Distance Regression, Eq. (4.15), is a nonlinear optimization problem. There exist a number of methods for the solution of these problems, most (if not all) of which require the computation, either analytically or numerically, of the Jacobian. In the cases where an analytical form of the full Jacobian matrix can be derived, both the accuracy and convergence rate of the minimization scheme can be greatly improved.

The nonlinear optimization solver employed by this thesis is described at length in [30], and "the foundation for the algorithm is a stable and efficient trust-region Levenberg-Marquardt minimizer that exploits the particular structure of the Jacobian of the orthogonal distance regression problem." The Levenberg-Marquardt method starts with the steepest descent method and smoothly transitions to the Gauss-Newton method, where the steps s and t are simply added to β and δ , as the solution is approached (these steps are defined explicitly in Sec. 4.4.5). This method employs a "trust-region" strategy that reduces the step size in proportion to the confidence of a model of the objective function at the current iteration.

The Jacobian, $J \in \mathbb{R}^{(n+nm) \times (p+nm)}$, can be formed by taking the partials of the (weighted, in the general case) errors ϵ and δ with respect to the parameters β and δ as follows

$$J = \begin{bmatrix} \frac{\partial \epsilon_1}{\partial \beta_1} & \dots & \frac{\partial \epsilon_1}{\partial \beta_p} & \frac{\partial \epsilon_1}{\partial \delta_1} & \dots & \frac{\partial \epsilon_1}{\partial \delta_{nm}} \\ \vdots & \ddots & \vdots & \vdots & \ddots & \vdots \\ \frac{\partial \epsilon_n}{\partial \beta_1} & \dots & \frac{\partial \epsilon_n}{\partial \beta_p} & \frac{\partial \epsilon_n}{\partial \delta_1} & \dots & \frac{\partial \epsilon_n}{\partial \delta_{nm}} \\ \frac{\partial \delta_1}{\partial \beta_1} & \dots & \frac{\partial \delta_1}{\partial \beta_p} & \frac{\partial \delta_1}{\partial \delta_1} & \dots & \frac{\partial \delta_1}{\partial \delta_{nm}} \\ \vdots & \ddots & \vdots & \vdots & \ddots & \vdots \\ \frac{\partial \delta_{nm}}{\partial \beta_1} & \dots & \frac{\partial \delta_{nm}}{\partial \beta_p} & \frac{\partial \delta_{nm}}{\partial \delta_1} & \dots & \frac{\partial \delta_{nm}}{\partial \delta_{nm}} \end{bmatrix}. \quad (4.20)$$

Note that the appearance of δ in both the errors and the parameters gives a special and exploitable structure to the Jacobian matrix. The Jacobian matrix can be divided into four block elements where all but the upper left block possess a special structure. These block elements are

labeled as follows

$$J = \begin{bmatrix} G & V \\ Z & D \end{bmatrix}. \quad (4.21)$$

G is the Jacobian matrix of ϵ with respect to β and has no special properties. V is the Jacobian matrix of ϵ with respect to δ and is a diagonal matrix. Z is the Jacobian matrix of δ with respect to β and is all zeros because δ is independent of β . D is the Jacobian of δ with respect to δ and is a diagonal matrix (in the constant-weight case, $D \neq I$). In a naive algorithm for ODR each element of V and D must be calculated. The time complexity for this calculation is $O(n^2 + np)$ (for the case of $m = 1$) where n is the number of observed data points. By exploiting the structure of the ODR problem, only the diagonal elements of V and D need to be calculated, reducing the time complexity from quadratic $O(n^2 + np)$ to linear $O(2n + np)$, a significant improvement.

In general, the block elements, G , V , D , of the Jacobian have the following form

$$G \in \mathbb{R}^{n \times p} : \quad G_{ij} = \frac{\partial f(\mathbf{X}_i + \boldsymbol{\delta}_i; \boldsymbol{\beta})}{\partial \beta_j}, \quad i = 1, \dots, n, \quad j = 1, \dots, p \quad (4.22a)$$

$$V \in \mathbb{R}^{n \times nm} : \quad V_{ij} = \frac{\partial f(\mathbf{X}_i + \boldsymbol{\delta}_i; \boldsymbol{\beta})}{\partial \delta_j}, \quad i = 1, \dots, n, \quad j = 1, \dots, nm \quad (4.22b)$$

$$D \in \mathbb{R}^{nm \times nm} : \quad D = \text{diag}\{w_i D_i, \quad i = 1, \dots, nm\} \quad (4.22c)$$

Let us now explicitly define the block elements of the Jacobian for the 3D body-frame linear velocity estimation ODR problem, given by Eq. (4.19). Each element of every row of $G \in \mathbb{R}^{n \times p}$ will have the following form

$$G_{i1} = w_i \frac{\partial \epsilon_i}{\partial v_x} = w_i [\cos(\theta_i + \delta\theta_i) \cos(\phi_i + \delta\phi_i)] \quad (4.23a)$$

$$G_{i2} = w_i \frac{\partial \epsilon_i}{\partial v_y} = w_i [\sin(\theta_i + \delta\theta_i) \cos(\phi_i + \delta\phi_i)] \quad (4.23b)$$

$$G_{i3} = w_i \frac{\partial \epsilon_i}{\partial v_z} = w_i [\sin(\phi_i + \delta\phi_i)]. \quad (4.23c)$$

For the case of $m > 1$ as in the case of the Doppler velocity ODR problem, $V \in \mathbb{R}^{n \times nm}$ can be shown to have the following "staircase" structure.

$$V = \begin{bmatrix} XX & & & \\ & XX & & \\ & & \ddots & \\ & & & XX \end{bmatrix} = \begin{bmatrix} V_1 & & & \\ & V_2 & & \\ & & \ddots & \\ & & & V_n \end{bmatrix}, \quad V_i \in \mathbb{R}^{1 \times m} = \begin{bmatrix} V_{i1} & V_{i2} \end{bmatrix} \quad (4.24)$$

Each of the $m = 2$ elements of each row of V will have the following form

$$V_{i1} = w_i \frac{\partial \epsilon_i}{\partial \theta_i} = w_i [-v_x \sin(\theta_i + \delta\theta_i) \cos(\phi_i + \delta\phi_i) + v_y \cos(\theta_i + \delta\theta_i) \cos(\phi_i + \delta\phi_i)] \quad (4.25a)$$

$$V_{i2} = w_i \frac{\partial \epsilon_i}{\partial \phi_i} = w_i [-v_x \cos(\theta_i + \delta\theta_i) \sin(\phi_i + \delta\phi_i) - v_y \sin(\theta_i + \delta\theta_i) \sin(\phi_i + \delta\phi_i) + v_z \cos(\phi_i + \delta\phi_i)]. \quad (4.25b)$$

Finally, $D \in \mathbb{R}^{nm \times nm}$ is composed of weighted block diagonal elements of the target-independent error variance ratio matrix such that

$$D = \begin{bmatrix} D_1 & & & \\ & D_2 & & \\ & & \ddots & \\ & & & D_n \end{bmatrix}, \quad D_i \in \mathbb{R}^{m \times m} = w_i \begin{bmatrix} \frac{\sigma_{vr}}{\sigma_\theta} & 0 \\ 0 & \frac{\sigma_{vr}}{\sigma_\phi} \end{bmatrix} \quad (4.26)$$

4.4.4 Computation of the Asymptotic Covariance Matrix

The calculation of the asymptotic covariance matrix is necessary to construct approximate confidence bounds around the point estimate of the model parameters provided by ODR [3]. A measure of uncertainty in the parameter estimate will be necessary for any type of sensor fusion technique that will incorporate the body-frame linear velocity vector measurement described by this thesis, in particular the visual-inertia-radar SLAM technique (VID-SLAM) developed by Stahoviak

and Kramer et al. [27]. Let us revisit the construction of the Jacobian matrix J . First, we construct the weighted residual vector $\mathbf{g}(\boldsymbol{\eta}) : \mathbb{R}^{p+nm} \rightarrow \mathbb{R}^{n+nm}$ as

$$g_i(\boldsymbol{\eta}) = \begin{cases} w_i [f(\mathbf{X}_i + \boldsymbol{\delta}_i; \boldsymbol{\beta}) - v_{r,i}] & i = 1, \dots, n \\ w_{i-n} d_{11} \delta_{i-n} & i = n+1, \dots, 2n \\ w_{i-2n} d_{22} \delta_{i-n} & i = 2n+1, \dots, n+nm, \end{cases} \quad (4.27)$$

where $\boldsymbol{\eta} = [\boldsymbol{\beta}, \boldsymbol{\delta}]^T$. The weighted ODR problem defined by Eq. (4.19) can now be re-written as

$$\boldsymbol{\eta}^* = \arg \min_{\boldsymbol{\eta}} \|\mathbf{g}(\boldsymbol{\eta})\|^2 = \arg \min_{\boldsymbol{\beta}, \boldsymbol{\delta}} \sum_{i=1}^{n+nm} [g_i(\boldsymbol{\beta}, \boldsymbol{\delta})]^2 \quad (4.28)$$

Let $J \in \mathbb{R}^{(n+nm) \times (p+nm)}$ denote the Jacobian of $\mathbf{g}(\boldsymbol{\eta})$, where

$$J_{ij} = \frac{\partial g_i}{\partial \eta_j} = \begin{bmatrix} G & V \\ Z & D \end{bmatrix} \quad (4.29)$$

has block elements defined by Eq. 4.22c. The asymptotic covariance matrix can now be defined as follows

$$\boldsymbol{\Sigma} = \left(\frac{1}{n+p} \right) \mathbf{g}^T \mathbf{g} (J^T J)^{-1} = \begin{bmatrix} \boldsymbol{\Sigma}_{\boldsymbol{\beta}} & \boldsymbol{\Sigma}_{\boldsymbol{\beta}\boldsymbol{\delta}} \\ \boldsymbol{\Sigma}_{\boldsymbol{\delta}\boldsymbol{\beta}} & \boldsymbol{\Sigma}_{\boldsymbol{\delta}} \end{bmatrix} \quad (4.30)$$

Typically only the upper $p \times p$ block of the covariance matrix is of interest to us as it represents the weighted uncertainty in the point estimate of the model parameters $\boldsymbol{\beta}$. Boggs and Rogers provide an efficient method for computing only this upper $p \times p$ block in [3].

The scaled covariance bounds are shown in Fig. 4.4. In this figure the $k\sigma$ envelope around the point estimate of the model parents is shown for $k = 10$. In Fig. 4.5, the true values of σ_{v_x} and σ_{v_y} are shown. In general, for the case of 2D radar data (no elevation information), the uncertainty in the estimate of v_x is smaller than uncertainty in the estimate of v_y , $\sigma_{v_x} < \sigma_{v_y}$.

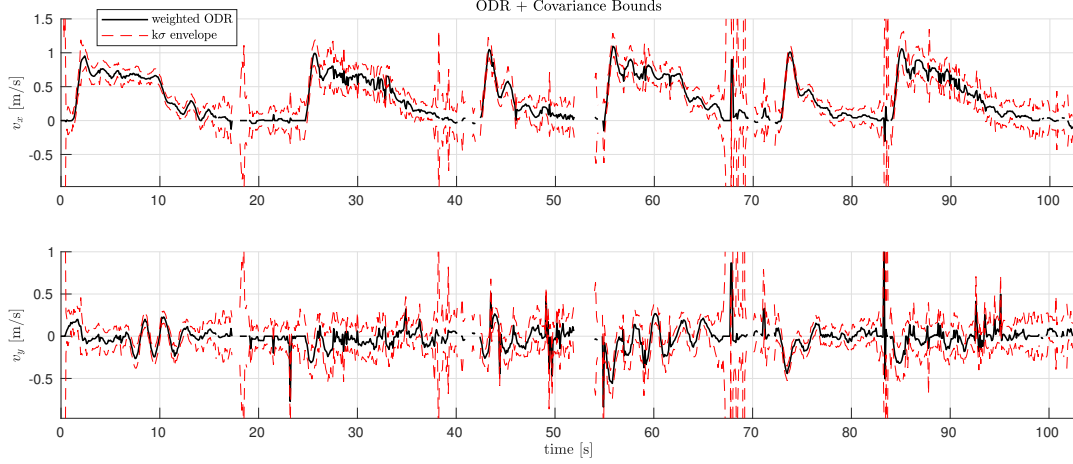


Figure 4.4: 2D Orthogonal Distance Regression (ODR) $k\sigma$ confidence bounds.

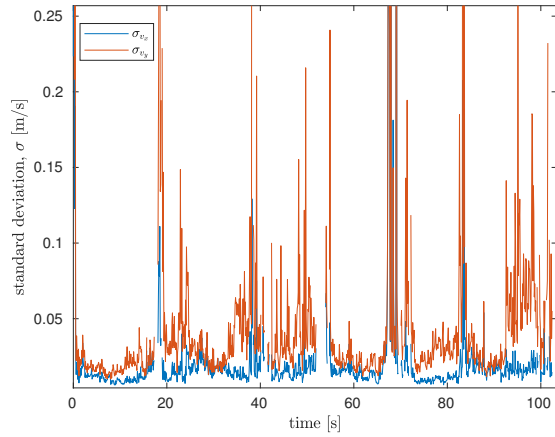


Figure 4.5: 2D Orthogonal Distance Regression (ODR) covariance values, $[\sigma_{v_x}, \sigma_{v_y}]$.

4.4.5 The ODR Algorithm

The implementation of ODR is summarized by the following algorithmic pseudocode. ODR is seeded with an initial guess of the model parameter vector given by the MLSESAC solution, and proceeds according to the following algorithm [30] until convergence.

Algorithm 1: Orthogonal Distance Regression, ODR

Data: β_0 seed from MLESAC, $\delta_0 \sim \mathcal{N}(0, \sigma_\theta)$ **Result:** ODR estimate of the model parameters β initialization: $s_0 \leftarrow \mathbf{1}_{px1}$ **while** $s <$ convergence criteria **do** Compute G , V and D — the block elements of the Jacobian of the objective function J

as described above.

 $P = V^T V + D^2 + \alpha T^2$ is defined to simplify the following equations, α is the Lagrange multiplier and T is the scaling matrix for t . Update the residual vector ϵ

$$\epsilon_i = v_x \cos(\theta_i + \delta\theta_i) \cos(\phi_i + \delta\phi_i) + v_y \sin(\theta_i + \delta\theta_i) \cos(\phi_i + \delta\phi_i) + v_z \sin(\phi_i + \delta\phi_i) - v_{r,i}$$

 based on the parameter estimate β_c , δ_c at the current iteration.

Formulate the unconstrained linear least squares problem from the linearization of the objective function (given by Eq. 4.19).

$$\min_s \left\| ((I - VP^{-1}V^T)^{1/2}Gs) - (I - VP^{-1}V^T)^{-1/2}(-\epsilon + VP^{-1}(V^T\epsilon + D\delta)) \right\|^2$$

 and solve for s .

$$\mathbf{t} = -P^{-1}(V^T + D\delta + V^T G s)$$

 Use s and t to update β and δ , respectively

$$\begin{bmatrix} \beta \\ \delta \end{bmatrix} = \begin{bmatrix} \beta_c \\ \delta_c \end{bmatrix} + \begin{bmatrix} S & \mathbf{0} \\ \mathbf{0} & T \end{bmatrix} \begin{bmatrix} s \\ t \end{bmatrix}$$

 where S and T can be user-defined or set according to the ODRPACK User Guide [?].**end**

Chapter 5

Results

Two series of studies are conducted to evaluate the proposed 3D body-frame velocity vector measurement algorithm for both simulated data and real-world experimental data collected onboard the ground and aerial vehicle platforms shown in Fig. 5.1. The real-world experimental datasets demonstrate results for both 2D and 3D velocity estimation. In both the 2D and 3D cases, the output of the velocity measurement algorithm is compared against a motion capture based estimation of groundtruth.



Figure 5.1: Experimental vehicle platforms with custom sensor rigs consisting of 77–81 GHz FMCW radar, Intel RealSense camera and microstrain IMU.

5.1 Simulation Study

In the simulation study, a set of radar measurements consisting of multiple targets and their corresponding Doppler velocities ($\theta_i, \phi_i, v_{r,i}$) were generated with Gaussian measurement noise

proportional to the known sensor specifications, $\sigma_{v_r} = 0.044$ m/s, $\sigma_\theta = 2.44^\circ$ and $\sigma_\phi = 2.36^\circ$. A subset of these target's Doppler measurements were corrupted with Gaussian white noise distributed as $\mathcal{N}(0, \sigma_{v_r} = 1.5$ m/s) in order to simulate outliers in the data as is typical for Doppler radar measurements. First, MLESAC is used to determine the set of inlier targets and a first-pass estimate of the velocity profile parameters. Then, both ODR and OLS are seeded with the MLESAC solution as an initial guess, and ODR is evaluated against the standard OLS solution for the inlier set.

Table 5.1: Simulation Study — Velocity Profile Estimation

Method	forward velocity v_x [m/s]	lateral velocity v_y [m/s]	vertical velocity v_z [m/s]	RMSE
truth	2.3200	-1.3300	-1.5200	—
MLESAC + OLS	2.2571	-1.2850	-1.6217	0.0738
MLESAC + ODR	2.3150	-1.3310	-1.5279	0.0054

In Fig. 5.2, it can be seen that targets appropriately classified as inliers will lie on or very near the true velocity profile surface, while appropriately rejected outliers will lie farther from the surface. Given the appropriately classified set of inlier targets, the ODR method achieves a velocity profile estimate that is an *order of magnitude improvement* over the OLS estimate.

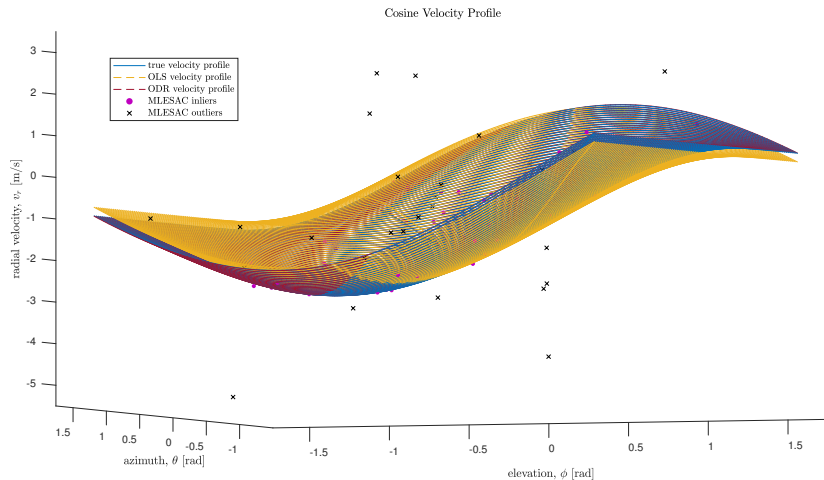


Figure 5.2: MLESAC outlier rejection and ODR velocity profile estimation

5.2 2D Radar Data - Static Environment

The formulation of the velocity vector measurement algorithm described in Ch. 4 is described for 3D radar data, but this method can easily be re-worked for the case of 2D radar data. In fact, this work on 2D radar data preceded the development of the 3D velocity vector measurement algorithm, but was left out of the formulation in Ch. 4 because of various aspects that would have been redundant in the 3D case.

Given that the detection plane of the sensor is rigidly aligned with the body-frame x-y plane, the proposed velocity profile measurement method is invariant to the typical three dimensional motion that a quadrotor-type vehicle undergoes, i.e. the local pitch and roll of the vehicle has no effect on the quality of the velocity vector measurement.

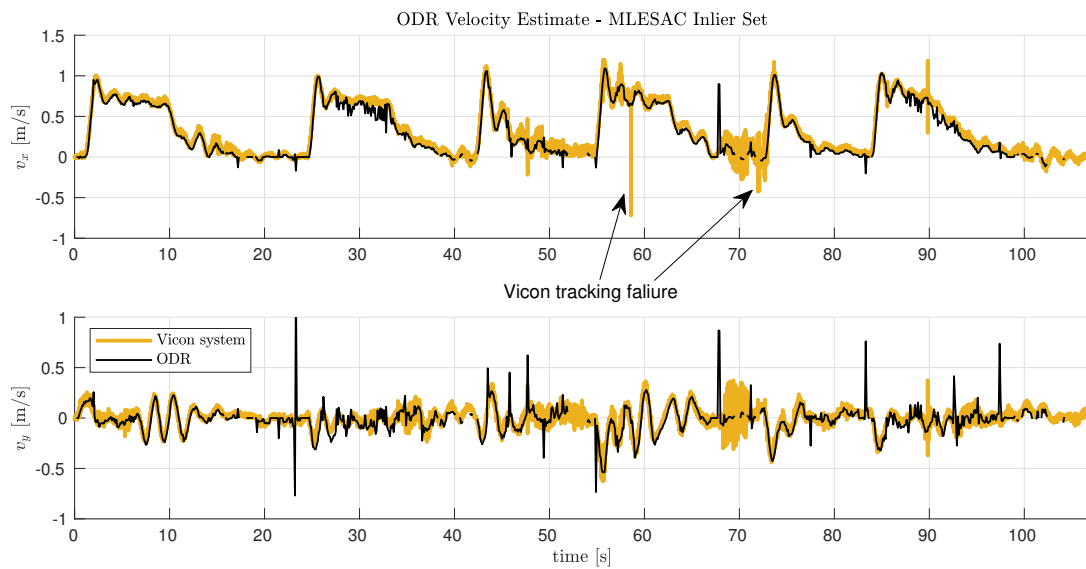


Figure 5.3: 2D Orthogonal Distance Regression (ODR) velocity vector measurement for a static environment. Also noted are time at which the Vicon motion-capture system is momentarily unreliable.

A comparison of the MLESAC, (constant weight) ODR, and intensity-weighted ODR velocity profile estimation methods for a real data set containing outliers in the form of noisy targets is given in Tab. 5.2.

Table 5.2: 2D Radar Data — Static Environment

Method	forward velocity, v_x RMSE [m/s]	lateral velocity, v_y RMSE [m/s]	Computational Cost
MLESAC	0.0981	0.1084	-
ODR	0.0811	0.0935	$O(np^2)$
weighted ODR	0.0712	0.0815	$O(np^2)$

5.3 2D Radar Data — Semi-dynamic Environment

In autonomous navigation and exploration tasks it is often the case that the vehicle’s environment is not entirely static, and in general we would like the velocity measurement method to be robust to a certain degree of dynamics in the scene. Given a single, forward-facing sensor, it has been shown that the velocity measurement algorithm proposed is robust to environment dynamics for scenarios in which dynamic agents do not dominate the target set for a given scan, i.e. the velocity vector hypothesis associated with the set of static targets must have a higher data log likelihood score than the hypothesis associated with any other group of dynamic targets. This implies that the set of static targets comprise a plurality of targets in any given scan.

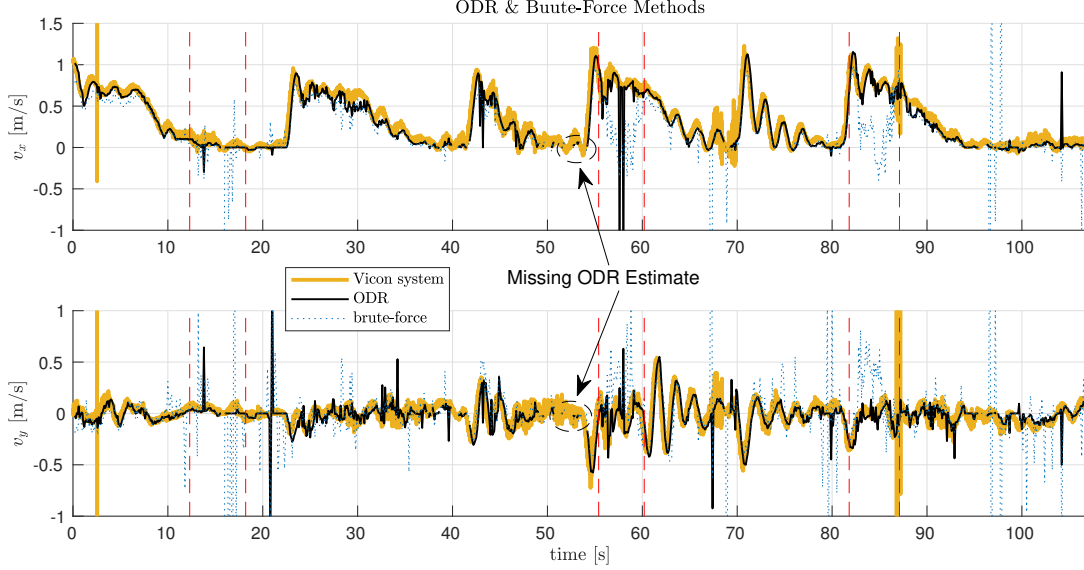


Figure 5.4: 2D Orthogonal Distance Regression (ODR) velocity vector measurement for a semi-dynamic environment. Dashed red lines – – indicate time intervals during which a person was moving in the scene.

At this point, a *brute-force* parameter estimation method is introduced for 2D radar data in order to make a comparison between two methods: one sensitive to outliers (the brute-force estimation scheme), and the other robust to the presence of outliers in the data (the MLESAC + ODR estimation scheme). The brute-force parameter estimation approach solves the uniquely-determined problem for *every* pair of targets (i, j) in the scan such that $\theta_i \neq \theta_j$.

$$\begin{bmatrix} v_x \\ v_y \end{bmatrix}_{ij} = \begin{bmatrix} \cos \theta_i & \sin \theta_i \\ \cos \theta_j & \sin \theta_j \end{bmatrix}^{-1} \begin{bmatrix} v_{r,i} \\ v_{r,j} \end{bmatrix} \quad (5.1)$$

Due to binning in range, angle and doppler space, it will be almost guaranteed that some subset of the targets in a particular scan satisfy $\theta_i = \theta_j$. Computationally, this will cost $O((n - 1)n/2)$ calculations per scan. After discarding outliers in the parameter estimate (2σ outliers perhaps), the brute-force parameter estimate can be given as

$$\begin{bmatrix} v_x \\ v_y \end{bmatrix}^* = \sum_{i=1}^{n-1} \sum_{j=i+1}^n w_{ij} \begin{bmatrix} v_x \\ v_y \end{bmatrix}_{ij} \Bigg/ \sum_{i=1}^{n-1} \sum_{j=i+1}^n w_{ij} \quad (5.2)$$

At three different times during the test, a person was moving in the scene among a number of static obstacles – this is indicated in Fig. 5.4 by the time intervals marked with dashed red lines. As seen in Fig. 5.4, the brute-force estimate is significantly degraded in the presence of dynamic elements with a *maximum deviation from ground truth of 1.14 m/s* in v_x during the third such interval. Though the brute-force estimate becomes unreliable, the MLESAC outlier rejection method is successful in removing dynamic targets from the data, and a robust estimate of the body-frame velocity profile can be derived from the MLESAC inlier set using ODR. During that same interval, the ODR velocity profile estimate resulted in an RMSE value of only 0.13 m/s in v_x and 0.16 m/s in v_y .

Table 5.3: 2D Radar Data — Semi-Dynamic Environment

Method	forward velocity, v_x RMSE [m/s]	lateral velocity, v_y RMSE [m/s]	Computational Cost
brute-force	0.3683	0.4107	$O(n^2/2)$
MLESAC	0.1540	0.1951	-
ODR	0.1118	0.1225	$O(np^2)$
weighted ODR	0.0906	0.1081	$O(np^2)$

5.4 3D Radar Data — Static Environment

Next, the proposed velocity measurement algorithm is evaluated for the case of 3D radar pointcloud data in a test environment composed entirely of static targets. A single forward-facing sensor has been mounted to the front of the quadrotor aerial vehicle platform, and just as in the case for the 2D experimental data, the detection axes of the sensor have been rigidly aligned with the body-frame axes of the vehicle. In the 3D configuration, the radar has a field-of-view (FOV) of approximately ± 75 degrees azimuth and ± 20 degrees elevation.

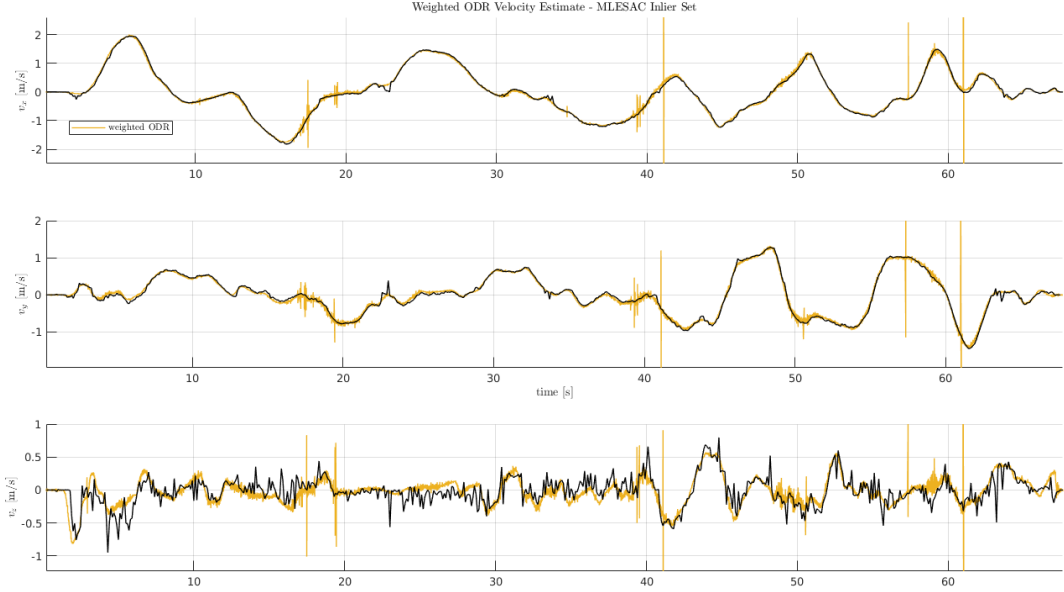


Figure 5.5: 3D Orthogonal Distance Regression (ODR) velocity vector measurement for a static environment.

It can be seen in Fig. 5.5 that the proposed method is able to recover a reliable measurement of both the v_x and v_y components of the 3D body-frame velocity vector. At times when the velocity measurement becomes unreliable (at approximately 23s, 34s and 63s into the test) the relative uncertainty in one or more of the measured velocity components increases proportionately. This is measured directly by the diagonal terms of the covariance matrix plotted in Fig. 5.6.

Table 5.4: 3D Radar Data — Static Environment

Method	forward velocity, v_x RMSE [m/s]	lateral velocity, v_y RMSE [m/s]	vertical velocity, v_z RMSE [m/s]
weighted ODR	0.0578	0.0619	0.1542

It is important to note the general trend in the diagonal entries of the covariance matrix, the relative uncertainties in the measurement of each of the three body-frame velocity components, that is

$$\sigma_{v_x} < \sigma_{v_y} < \sigma_{v_z}$$

This relative magnitude agrees with the RMSE values reported in Tab. 5.4. If the measurement of the component of the velocity vector that is aligned with the forward direction (sensor x-axis) of the sensor has the lowest associated measure of uncertainty, then these two figures make a compelling case for the addition of multiple radar sensors each aligned with one of the body-frame axes. Via a sensor fusion technique, measurements of the body-frame velocity vector components can be combined using their associated covariance values, and an improved radar-only velocity measurement algorithm could be developed. This idea will be discussed further in Ch. 5.

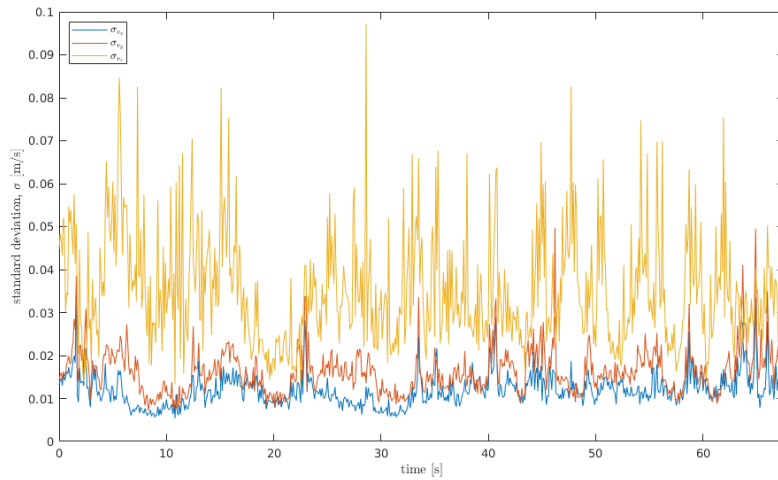


Figure 5.6: 3D Orthogonal Distance Regression (ODR) measurement uncertainties

Chapter 6

Conclusion

This thesis described a method by which an instantaneous measurement of the 3D body-frame linear velocity components of a sensor platform equipped with a single axes-aligned radar sensor can be derived. The accuracy of the proposed method was validated for both simulated and experimental radar data, and was shown to be robust to sensor noise, environment dynamics, and other processes by which radar data can be corrupted, e.g. binning of discrete FFT data and multipath reflections. This method makes the following contributions to the field of robust ego-motion estimation:

- (1) Development of a robust, radar-based, model-free 3D ego-velocity measurement method.

The proposed methods operates solely on radar target data, and does not require a motion or vehicle dynamics model.

- (2) An instantaneous measurement of the sensor platform's ego-velocity is produced at the frame rate of the sensor (10Hz) without requiring input from additional sensors or any form of temporal filtering of data and measurements from previous scans.

- (3) By producing an estimate of the measurement uncertainty in the form of the measurement covariance matrix, the proposed ego-velocity measurement can be effectively fused into any number of sensor fusion based estimation schemes, in particular the author has in mind a visual-inertial-radar SLAM system.

In addition to the strengths of the proposed method, it is important to understand where there is room for improvement on the work described thus far. There are several avenues for improvement of the ego-velocity measurement algorithm described by this thesis that I would like to briefly summarize here.

- (1) **Multi-radar sensor fusion:** It was shown in Ch. 5.4 that the relative uncertainty in the measurement of the ego-velocity vector components was such that $\sigma_{v_x} < \sigma_{v_y} < \sigma_{v_z}$. In this case, the x-axis of the sensor is normal to the patch-antenna array and was aligned with the x-axis of the vehicle. The author imagines a logical extension of this method by which multiple (up to three) radar sensors, each aligned with a single body-frame axis of the vehicle, could be fused to improve the measurement of all three components, and especially improve the noticeably noisy measurement of v_z .
- (2) **Multi-sensor fusion:** Another method by which the relatively poor estimate of v_z could be improved is via a multi-sensor fusion approach. As can be seen in Fig. 5.5, the estimate of v_z is not a reliable estimate of the true vertical component of the platform's body-frame velocity vector, and this is reflected by the uncertainty, σ_{v_z} , associated with the estimated v_z component. One method for improving the measurement of v_z (as well as the measurement of the v_x and v_y components) would be to incorporate acceleration constraints between radar frames in the form of measurements of linear and angular accelerations from an inertial measurement unit (IMU).
- (3) **Sliding-window filter:** A form of sliding-window filter could be used to incorporate velocity estimates from previous scans into the velocity estimate of the current scan. Posing the 3D body-frame ego-velocity estimation problem as a nonlinear optimization problem over the last N radar frames and their associated IMU measurements could be used to derive the most accurate possible estimate of the sensor platform's 3D ego-velocity vector. This method would necessarily incorporate item (2), and possibly item (1).

- (4) **Bayesian Nonlinear Regression:** It is important to revisit the assumption of Gaussian errors associated with the measurements of range, azimuth, elevation and Doppler velocity for each target that the radar produces. Orthogonal Distance Regression is a maximum likelihood method. This necessarily implies the assumption of Gaussian noise processes associated with the observations of both the *explanatory* and *dependent* variables, $[\theta_i, \phi_i]^T$ and $v_{r,i}$, respectively. However, the binning process associated with the discrete FFTs that calculate range, angle-of-arrival and Doppler velocity are not Gaussian by nature. A visualization of the azimuth angle bins is shown in Fig. ???. Having an informed understanding (via a radar calibration process perhaps) of a distribution that more realistically models the errors associated with the radar binning process could lead to a more accurate estimate of the 3D ego-velocity vector. Knowledge of this distribution could be folded into a Bayesian Nonlinear Regression framework by way of introducing a prior on the distribution from which radar errors are sampled.

Bibliography

- [1] G. Allibert, D. Abeywardena, M. Bangura, and R. Mahony. Estimating body-fixed frame velocity and attitude from inertial measurements for a quadrotor vehicle. In 2014 IEEE Conference on Control Applications (CCA), pages 978–983, Oct 2014.
- [2] P. Boggs, R. Byrd, and R. Schnabel. A stable and efficient algorithm for nonlinear orthogonal distance regression. SIAM Journal on Scientific and Statistical Computing, 8(6):1052–1078, 1987.
- [3] Paul T. Boggs and Janet E. Rogers. The computation and use of the asymptotic covariance matrix for measurement error models. Technical report, National Institute of Standards and Technology, 1989.
- [4] Paul T. Boggs and Janet E. Rogers. Orthogonal distance regression. Technical report, National Institute of Standards and Technology, 1989.
- [5] G. Brooker, R. Hennessey, C. Lobsey, and M. Bishop. Seeing through dust and water vapor: millimeter wave radar sensors for mining applications. In Journal of Field Robotics, volume 27, pages 527–557, July 2007.
- [6] Michael Burri, Janosch Nikolic, Pascal Gohl, Thomas Schneider, Joern Rehder, Sammy Omari, Markus W Achtelik, and Roland Siegwart. The euroc micro aerial vehicle datasets. The International Journal of Robotics Research, 2016.
- [7] Feng Cao, Martin Estert, Weining Qian, and Aoying Zhou. Density-Based Clustering over an Evolving Data Stream with Noise, pages 328–339.
- [8] S. Cen and P. Newman. Precise ego-motion estimation with millimeter-wave radar under diverse and challenging conditions. In 2018 IEEE International Conference on Robotics and Automation (ICRA), page to appear, May 2018.
- [9] J. Dickmann, N. Appenrodt, H. Bloecher, C. Brenk, T. Hackbarth, M. Hahn, J. Klappstein, M. Muntzinger, and A. Sailer. Radar contribution to highly automated driving. In 2014 44th European Microwave Conference, pages 1715–1718, Oct 2014.
- [10] Martin Ester, Hans-Peter Kriegel, Jörg Sander, and Xiaowei Xu. A density-based algorithm for discovering clusters in large spatial databases with noise. In Proceedings of the Second International Conference on Knowledge Discovery and Data Mining, KDD’96, pages 226–231. AAAI Press, 1996.

- [11] Robert Ferguson, Matthieu Chevrier, and Alan Rankin. mmwave radar: Enabling greater intelligent autonomy at the edge. Technical report, Texas Instruments, 2018.
- [12] Martin A. Fischler and Robert C. Bolles. Random sample consensus: A paradigm for model fitting with applications to image analysis and automated cartography. *Commun. ACM*, 24(6):381–395, June 1981.
- [13] Christian Forster, Luca Carlone, Frank Dellaert, and Davide Scaramuzza. On-Manifold Preintegration for Real-Time Visual–Inertial Odometry. *IEEE Transactions on Robotics*, 33(1):1–21, February 2017.
- [14] Wayne A Fuller. *Measurement Error Models*. John Wiley & Sons, Inc., New York, NY, USA, 1986.
- [15] V. Grabe, H. H. Blthoff, and P. R. Giordano. On-board velocity estimation and closed-loop control of a quadrotor uav based on optical flow. In *2012 IEEE International Conference on Robotics and Automation*, pages 491–497, May 2012.
- [16] D. Kellner, M. Barjenbruch, K. Dietmayer, J. Klappstein, and J. Dickmann. Instantaneous lateral velocity estimation of a vehicle using doppler radar. In *Proceedings of the 16th International Conference on Information Fusion*, pages 877–884, July 2013.
- [17] D. Kellner, M. Barjenbruch, J. Klappstein, J. Dickmann, and K. Dietmayer. Instantaneous ego-motion estimation using multiple doppler radars. In *2014 IEEE International Conference on Robotics and Automation (ICRA)*, pages 1592–1597, May 2014.
- [18] R. Mebarki, J. Cacace, and V. Lippiello. Velocity estimation of an uav using visual and imu data in a gps-denied environment. In *2013 IEEE International Symposium on Safety, Security, and Rescue Robotics (SSRR)*, pages 1–6, Oct 2013.
- [19] Fernando Nobre, Christoffer R. Heckman, and Gabe T. Sibley. Multi-sensor slam with online self-calibration and change detection. pages 764–774, 03 2017.
- [20] M. Rapp, K. Dietmeyer, M. Hahnand, and F. Schuster. Fscd and basd: Robust landmark detection and description on radar-based grids. In *International Conference on Microwaves for Intelligent Mobility (ICMIM)*, page to appear, 2016.
- [21] Mark A. Richards. *Fundamentals of Radar Signal Processing*. McGraw-Hill Professional, $\lfloor \text{country} \rfloor / \text{US} \rfloor / \text{country}$, 2005.
- [22] F. Schuster, C. G. Keller, M. Rapp, M. Haueis, and C. Curio. Landmark based radar slam using graph optimization. In *2016 IEEE 19th International Conference on Intelligent Transportation Systems (ITSC)*, pages 2559–2564, Nov 2016.
- [23] F. Schuster, M. Wrner, C. G. Keller, M. Haueis, and C. Curio. Robust localization based on radar signal clustering. In *2016 IEEE Intelligent Vehicles Symposium (IV)*, pages 839–844, June 2016.
- [24] Bruno Siciliano and Oussama Khatib. *Springer Handbook of Robotics*. Springer-Verlag, Berlin, Heidelberg, 2007.

- [25] R. Smith, M. Self, and P. Cheeseman. Estimating uncertain spatial relationships in robotics. In Proceedings. 1987 IEEE International Conference on Robotics and Automation, volume 4, pages 850–850, March 1987.
- [26] Randall C. Smith and Peter Cheeseman. On the representation and estimation of spatial uncertainty. Int. J. Rob. Res., 5(4):56–68, December 1986.
- [27] C. Stachowiak, A. Kramer, C. Williams, and C. Heckman. VID-SLAM: Visual-inertial SLAM with doppler radar based velocity constraints. In 2019 International Symposium on Robotics Research (ISRR), 2019, submitted.
- [28] S. Thrun and M. Montemerlo. The GraphSLAM algorithm with applications to large-scale mapping of urban structures. International Journal on Robotics Research, 25(5/6):403–430, 2005.
- [29] P.H.S. Torr and A. Zisserman. MLESAC: A new robust estimator with application to estimating image geometry. Computer Vision Image Understanding, 78(1):138–156, April 2000.
- [30] Jason W. Zwolak, Paul T. Boggs, and Layne T. Watson. Algorithm 869: Odrpack95: A weighted orthogonal distance regression code with bound constraints. ACM Trans. Math. Softw., 33:27, 2004.

Appendix A

Orthogonal Distance Regression, A Poem

Buried in the original NIST manuscript of '*A stable and Efficient Algorithm for Nonlinear Orthogonal Distance Regression*' [2] is the following poem. It's not easy to find the scanned copy of that original publication, so for posterity's sake, I'd like to repeat it here.

Orthogonal Distance Regression

When observations are corrupted
By errors random i.i.d.
Least Squares provides the answer
A true blue friend it be

But when the independents
In addition come unclean
Nonlinearities enter
And friends desert the scene

Now in your darkest hour
When hope is all but gone
This paper comes to show you
How estimation can go on

What is this shining hope
That beacon from afar?
Is it that new found wonder
That's known as ODR?

Yes! That's right! You've got it!
And we tell all below
From problem through solution
With codes that make it go

So calm your pounding heart
And mop your sweating brow
Your data can be handled
And we will show you how

Boggs, Byrd and Schnabel (1987)